Original Russian Text © A. E. Pogrebnoi, 2023,
published in MORSKOY GIDROFIZICHESKIY ZHURNAL, Vol. 39, Iss. 1 (2023)

Estimation of Internal Wave Parameters in the Arctic Based on Synthetic Aperture Satellite Radar Data

A. E. Pogrebnoi

Marine Hydrophysical Institute of RAS, Sevastopol, Russian Federation
✉ *pogrebok57@mail.ru*

Abstract
Purpose. The work is aimed at developing a technique for calculating the solitary internal wave parameters (solitons generated by a semi-diurnal tide) based on their manifestations on the ocean surface in the presence of ice.
Methods and Results. Sequential soundings of the *Sentinel*-1*A* and *Sentinel*-1*B* radar satellites west of the deep-sea part of the Fram Strait in August, 2018 were analyzed. Identification of the internal waves' surface manifestations on the radar satellite images is reduced to finding thin bright bands elongated along the wave crests. Bright pixels, the distance between which is less than the visual width of the ridges, are united into the clusters. The clusters whose sizes exceed the threshold value and for which the anisotropy (the ratio of the semi-axes of the approximating ellipse) is also high, are considered to correspond to the internal waves (in contrast to ice). For each such cluster, the interpolated spatial coordinates are calculated along the corresponding wave extremum. Based on the proposed method, the horizontal size ("wavelength" ~ 1.5 km) and the phase speed (~ 1 m/s) of solitary internal waves are assessed. The repetition period of solitons was ~ 24 min. The leading wave propagation speed appeared to be 10 % higher than that of the next one. During the time between soundings (~ 48 min), this leads to a "wavelength" increase (red shift) between them – from 1.3 to 1.6 km. The curvature radii' values of each wave front are also calculated. The information on spatial position of the fronts' curvature centers permits to assume the place of generation of the analyzed internal waves, namely the underwater bank (80° 45' N, 8° 30' W), the depth above which is less than 20 m.
Conclusions. The proposed method for identifying internal waves can be used to assess their kinematic and dynamic characteristics.

Keywords: internal waves, phase speed of internal waves, solitons, satellite radar images of the ocean surface, Fram Strait, Arctic

Acknowledgements: The study was financially supported by the Russian Science Foundation Grant No. 21-17-00278.

For citation: Pogrebnoi, A.E., 2023. Estimation of Internal Wave Parameters in the Arctic Based on Synthetic Aperture Satellite Radar Data. *Physical Oceanography*, 30(1), pp. 98-111. doi:10.29039/1573-160X-2023-1-98-111

DOI: 10.29039/1573-160X-2023-1-98-111

Introduction

The formation of weather and climate on our planet is determined by the World Ocean, solar radiation and atmosphere. On the one hand, the Sun and the Earth's atmosphere directly and indirectly have a decisive impact on all dynamic processes in the ocean. On the other hand, the World Ocean, in its turn, serves as a heat source that determines atmospheric circulation. The lack of balance between the influx of heat into the ocean and its outflow leads to the appearance of winds in the atmosphere.

An important element of the dynamic structure of the ocean is internal waves (IWs). They play a special role in the studies of the Arctic Basin. For example, the generation of internal waves by a barotropic tide over steep sections of

the continental slope leads to an intensification of turbulent mixing and stimulates heat transfer from the Atlantic waters to the surface [1], which significantly affects the climate system of the Arctic Ocean. IWs in the Arctic affect sea ice and the formation of polynyas [2–4].

Geographically, the seas of the Arctic Basin are located near the critical latitude [5–7]. Under these conditions, the dissipation of tides of semi-diurnal frequency leads to the formation of sets of short-period internal waves. These waves accumulate the energy of internal tides, transfer it during their propagation and gradually dissipate, mixing the waters.

The appearance of satellite monitoring data with high spatial resolution in open access has led to the intensification of IW studies in the ocean by remote methods. These methods are based on the study of surface manifestations of IWs on satellite images in the form of alternating light and dark bands [8–10]. On radar images of the sea surface, the light bands are rips (zones of convergence with intensification of surface waves), and dark bands are slicks (relatively smoothed divergence zones). For visible range data, on the contrary, the areas of increased roughness (rips) have lower brightness than slicks.

For analysis, both the data from satellites in the visible range [11–13] and the data from synthetic aperture radars (SAR) [14, 15] are used. Satellite information provides the estimation of the main spatial characteristics of internal waves: the wavelengths inside trains, the length of the crest of the leading wave, and the distances between successive packets (see, for example, [16, 17]). Over time, the shape and characteristics of IWs change. However, in the presence of quasi-synchronous soundings, when successive satellite images are taken with small time interval, one can try to determine the phase speeds of IWs [15, 18].

Unfortunately, currently there is no automatic identification of IWs. The process of determining IW parameters from satellite images is labor-intensive and subjective. This is due to the fact that possible manifestations of IWs are too diverse. It can be either a solitary soliton or a packet. The number of wave extremes in a packet can be various. The azimuthal orientation of the waves can also be various. It is still unknown how to automatically distinguish surface manifestations of waves from wakes, filaments, etc. Wave identification is hindered by the possible presence of third-party surface objects (for example, ice floes), and when using active SAR, coherent speckles.

The purpose of this work is to obtain objective generalized characteristics of internal waves generated by a semi-diurnal tide in the presence of ice floes in the area of their generation.

The used data

To calculate the characteristics of IW surface manifestations, we selected the data from Sentinel-1A and Sentinel-1B modern C-band radar satellites launched by the European Space Agency in 2014 and 2016, respectively. The Extra Wide Swath mode with a coverage bandwidth of 400 km and a spatial resolution of 40 × 40 m was applied. The period of obtaining information from each of these satellites in the equatorial zone is 12 days. However, due to the fact that the orbits are polar and the coverage band is wide, in the polar regions the frequency of measurements in the latitude band 70°÷85° increases up to four times a day.

Herewith, there are areas where the interval between successive scans of the Sentinel-1A and Sentinel 1B scanners is close to half of their orbital period (less than 50 min).

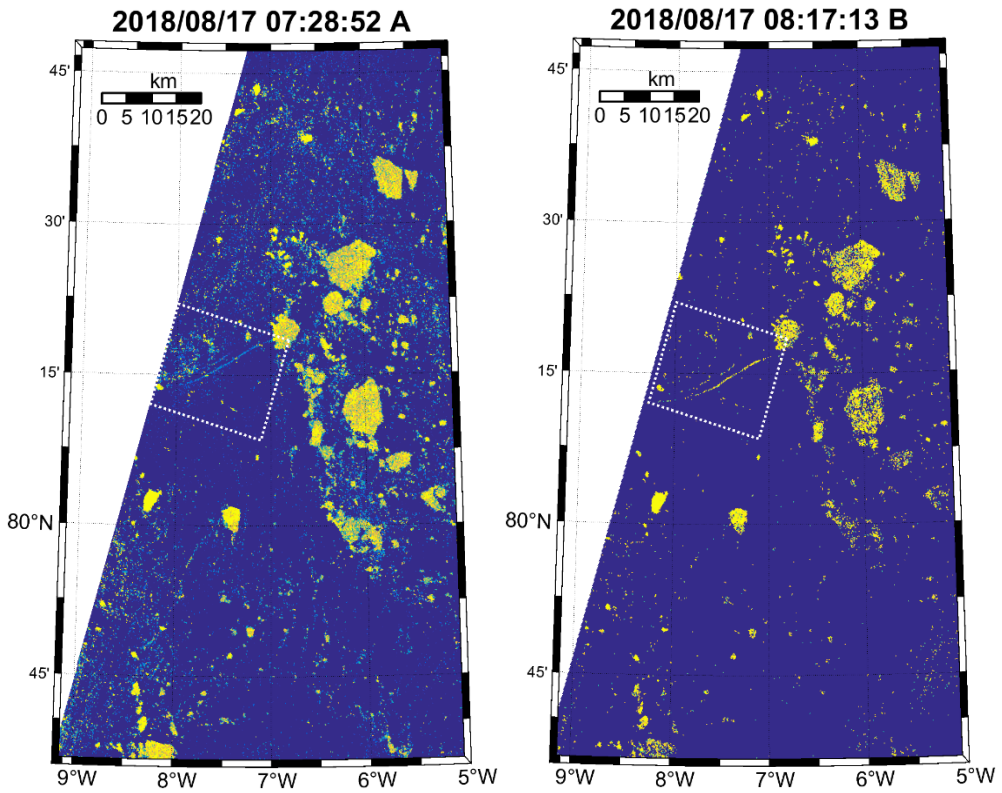

F i g. 1. Radar images of sea surface on August 17, 2018 (SAR Sentinel-1A and -1B). The dashed line shows a fragment with the IW surface manifestations

In this work, we analyzed a quasi-synchronous pair of Sentinel-1A and -1B satellite images taken on August 17, 2018 near the Fram Strait (Fig. 1). The time interval between soundings was 2901 s. Both images are cropped in space to the area of their mutual overlap. The dashed line highlights a fragment with surface manifestations of internal waves.

Identification of IW crests

During stratification above the unevenness of the bottom, the barotropic tide deforms the isopycnal surfaces and generates internal waves. An increase in the wave energy can cause its breaking and energy transfer to a packet of short-period internal waves [19].

The leading wave excited by the tide has the form of an impulse with downward deflection of isopycnal surfaces. The motion of such an impulse of deepening of isopycnal surfaces in the form of a single internal wave leads to

the formation of a convergent zone on the ocean surface [19]. Such convergent zones appear on radar images as light bands (rips).

Thus, the identification of IW surface manifestations in radar satellite images is reduced to finding thin light bands elongated along the leading IW crest. In this case, an internal wave crest is a position of the IW front above the deflection of isopycnal surfaces.

The procedure for identifying IW becomes much more complicated if there are external surface objects in the area of their manifestation, for example, ice floes. In addition, we note that, despite the compact spatial distribution of bright pixels belonging to a single IW crest, sometimes they do not touch each other. Therefore, a special masking procedure is also needed to combine such "related" pixels into a single cluster.

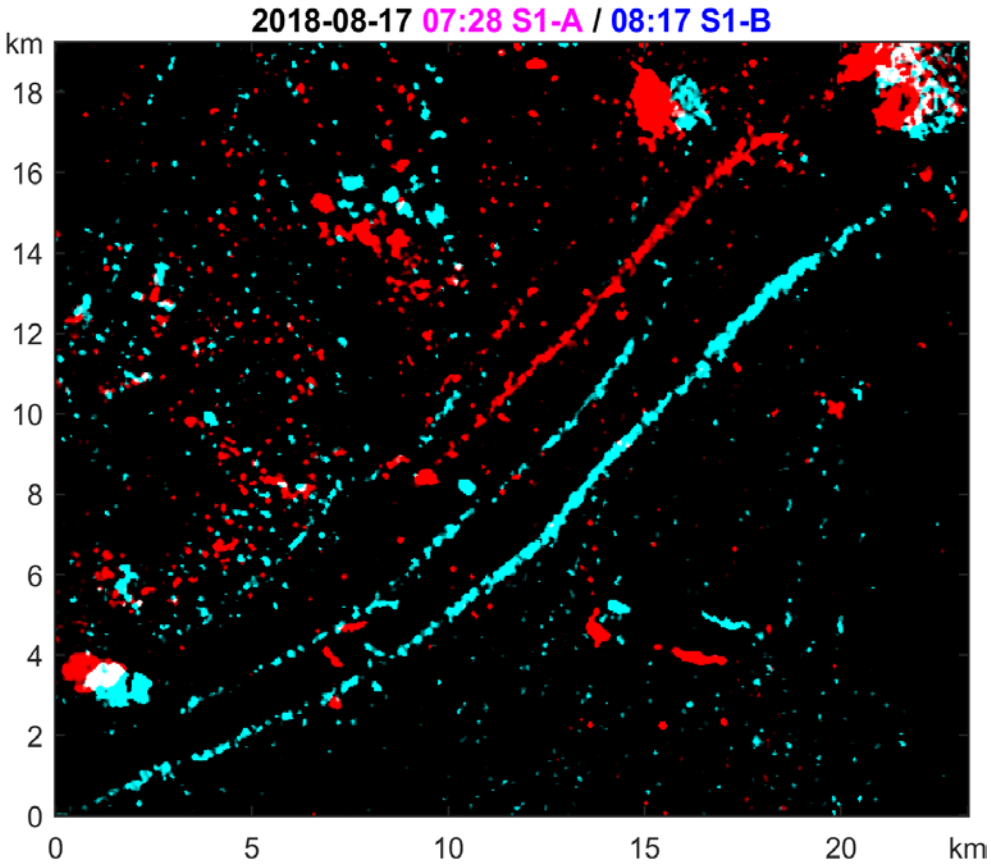

F i g. 2. Anaglyph of the sea surface images. Red gradations are used for the first sounding (Sentinel-1A), and blue-green tones are for the second one (Sentinel-1B)

Each satellite image has its own projection coordinates of the Earth's surface. Therefore, for analysis with joint processing, it is desirable to reduce the sounding data to a single coordinate system. When constructing maps in Fig. 1, Lambert Conformal Conic projection was applied. The fragment containing internal waves is marked with a dotted line. This fragment is given in Fig. 2 in the projection

coordinate system of Sentinel-1A satellite with the original pixel resolution (40 × 40 m). The image of Sentinel-1B satellite has been transformed into the same coordinate system. To jointly display both soundings in a single figure (Fig. 2), an anaglyph is used, when information fields of each satellite correspond to individual chromatic regions of the spectrum: red gradations for Sentinel-1A, and blue-green tones for Sentinel-1B. Axes are marked in kilometers.

Masking procedure

Thus, in Fig. 2, the surface manifestations of IWs are clusters of high-brightness pixels, elongated in the form of thin light bands, red for Sentinel-1A satellite and blue-green for Sentinel-1B. In addition to them, there are images of many ice floes of different sizes. The ice floes do not have a pronounced shape anisotropy in any direction. This is their main difference from the surface manifestations of IWs.

To separate the information related to IWs and other surface objects, and to combine the information for each IW crest into individual clusters, the following masking procedure was performed:

– for each sounding, the brightness range of the pixels of interest, characteristic of these clusters, was determined. Brightness values for points outside this range were set to zero;

– in order to combine closely located pixels into a single connected structure, a spatial mask was created for each sounding. To do this, each image was averaged with a spatial Gaussian filter with an arm exceeding the visual width of individual wave extrema (crests of internal waves);

– further, the obtained masks were binarized. All values exceeding the threshold were assigned ones, and the rest of the points were assigned zeros. To determine the threshold, the histogram method, which automatically chooses the threshold value to minimize the intraclass variance of the thresholded black and white pixels [20], was applied;

– the resulting BW-image was clustered: each individual cluster is a sub-region of the image formed by bright pixels touching each other;

– the pixel values in the clusters, the sizes of which are small, were reset to zero and repeated clustering was carried out. As a result, clusters with IWs and, possibly, several of the largest ice floes (up to three in our case) remained;

– to finally get rid of unwanted clusters, the fact that the manifestations of IWs are essentially anisotropic is used. Therefore, the shape of each cluster was approximated by an ellipse, and clusters with small values of the ratio of the major and minor semiaxes of the ellipse (less than 50) were eliminated;

– clusters with IWs were assigned identifiers *A/B* (satellite) and *n/s* (north/south wave extremum);

– the resulting masks were superimposed on the original images. Each filtered pixel was assigned an identifier corresponding to its cluster. The result is given in an anaglyph Fig. 3.

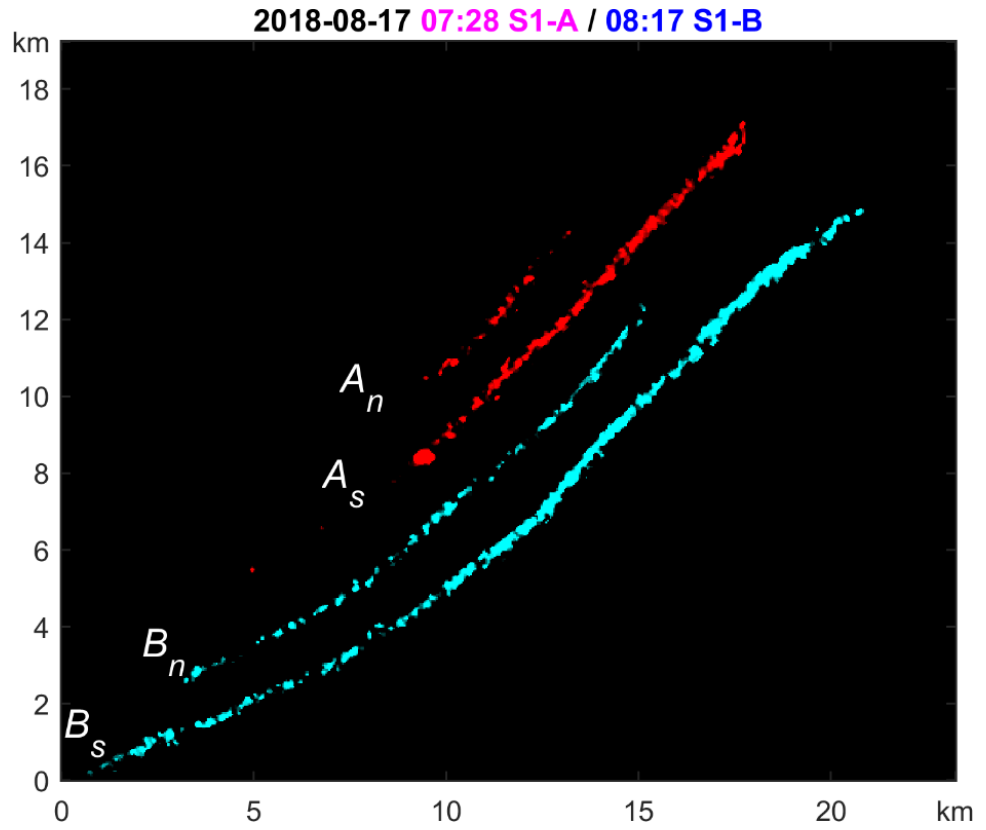

F i g. 3. Result of IW masking

Interpolation and smoothing

The obtained sets of points are scattered in the vicinity of wave fronts, and for each front we need objective along-frontal, preferably equidistant values of the coordinates $\{x_i,\ y_i\}$

Depending on the inclination angle in our wavefront coordinate system, the dependence $y = f(x)$ is not necessarily one-to-one. To ensure this uniqueness, it is convenient to pass to the oblique coordinate system $\{X', Y'\}$, in which the abscissa axis is directed along the previously calculated semi-major axis of the ellipse approximating the given cluster of points.

By the coordinate X', which we will consider as an argument, we sort the pairs $\{x_i',\ y_i'\}$. Then, separately for each x_i' and y_i', we perform parametric smoothing depending on the values of index i. To do this, we use a moving average filter with a robust version of the local regression based on polynomials of the 1st degree [21].

The resulting sets of coordinates are not equidistant. Therefore, the linear length of the front L is calculated from the distances l between adjacent coordinates along front, and the new values of the coordinates are interpolated in accordance with the equidistant values of the parameter l_i. Now the equidistant interpolated parametric coordinates of the wavefront can be returned to the original coordinate

system of the Sentinel-1A satellite image. The result of the wave extrema interpolation is given in Fig. 4, *a*.

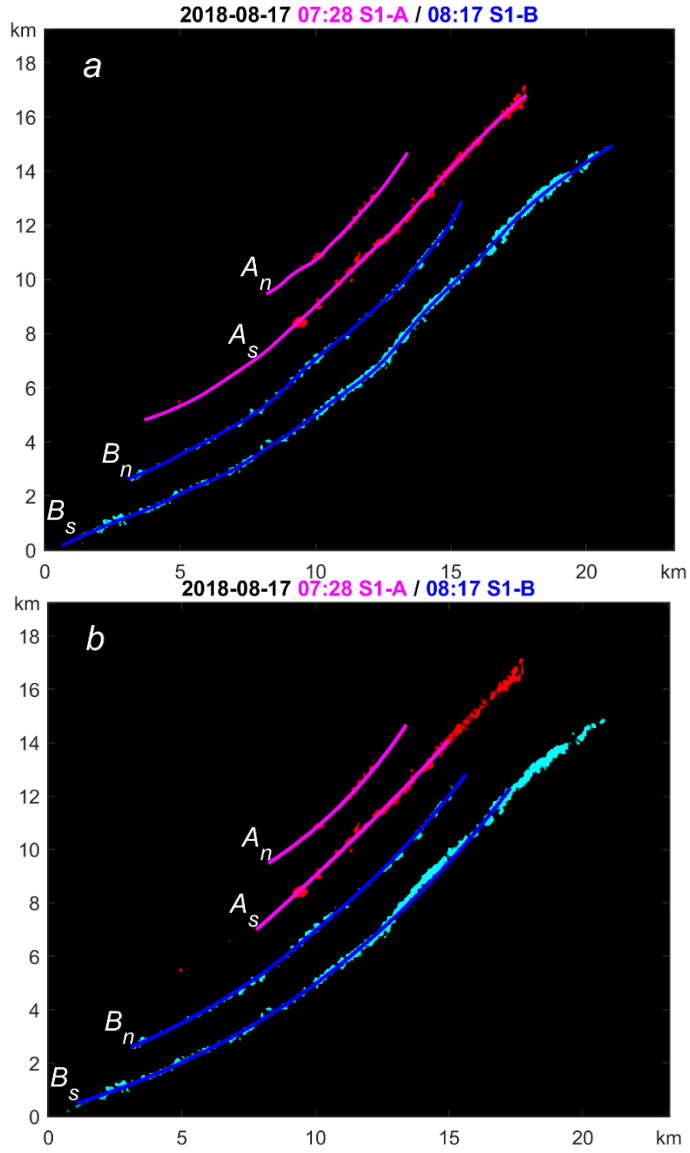

F i g. 4. Spatial interpolation of the wave front coordinates without smoothing (*a*) and with it (*b*) (along-frontal resolution is 40 m)

Along the wave front, its curvature can change locally, which affects the variability in calculating the distances between wave fronts, their propagation speed, and especially the radius of curvature. Therefore, the curves describing the fronts should be additionally smoothed. This will enable us to talk about the generalized values of the characteristics.

Each of the observed wave trains has its own along-frontal length, and to calculate the wavelengths and phase speed of their propagation, the information on the position of the fronts in places where both wave trains are present is required. Therefore, when calculating the smoothed characteristics of the position of the fronts, the edge sections that do not have such a correspondence were not taken into account.

Table 1 presents the linear lengths of the interpolated L_i and smoothed L_s sections of the wave fronts. The corresponding values of the number of pixel points in their calculation (N_i and N_s) and the corresponding length dispersions (σ_{Li} and σ_{Ls}) are also indicated there. In the calculations, the parametric coordinates $\{x_i,\ y_i\}$ with an equidistant resolution of 40 m were used. To identify the wave fronts, the identifiers of the corresponding clusters were used (*A*/*B* – satellite, *n*/*s* – north/south wave front). From the point of view of wave propagation direction, the southern front is the leading (first) one.

T a b l e 1

Assessment of the spatial position of wave fronts

Wave fronts	N_i	L_i , m	σ_{Li}, m	N_s	L_s, m	σ_{Ls}, m
A_s	5058	18693	144.7	2845	10092	142.1
A_n	1537	7446	122.7	1531	7372	124.4
B_s	4311	25455	108.8	3348	20438	136.2
B_n	1581	16356	78.2	1586	16371	95.4

The smoothing result is given in Fig. 4, *b*. The smoothed sets of wave front coordinates obtained in this way will be used in further calculations.

Parameters of wave fronts

Wavelength, phase speed and IW period

As noted above, all wave fronts have different along-front lengths. Therefore, the results of calculations of wavelengths λ and phase speeds *C* were carried out for zones in which all pairs of front points corresponding to each other are present. The shorter front determines the spatial range of the calculation of the phase speed of the northern (*n*) and southern (*s*) crests and wavelength during the first (*A*) and second (*B*) soundings. For each point of this shorter front, the distance to the nearest point on the second front corresponding to the computated parameter was calculated. Let us remind that all processed points are distributed uniformly along the fronts with an equidistant distance of 40 m. The spatial positions of fronts, wavelengths λ and phase speeds of wave extrema are given in Fig. 5.

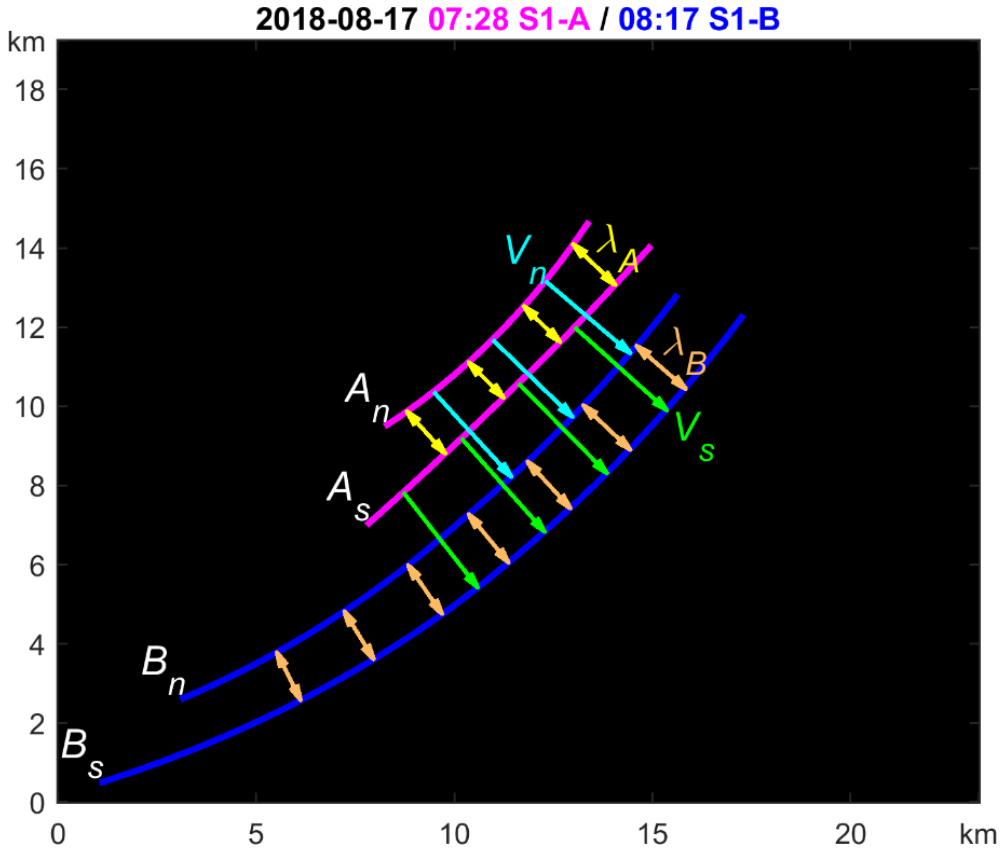

F i g. 5. Wavelengths λ and phase speeds *C* of the wave extrema

The average values $\overline{\lambda}$ and $\overline{C}$ and their dispersions σ_λ and σ_C are given in Tables 2 and 3. They were calculated in the usual way, the 95% confidence intervals for the variability of these wave characteristics were determined directly from the obtained samples, so as not to use the assumptions about the normality of distributions. Their estimates for λ and *C* are also given in Tables 2 and 3.

T a b l e 2

"Wavelengths" λ

Sounding	Average value of "wavelength" $\overline{\lambda}$, m	"Wavelength" dispersion σ_λ, m	95% confidential interval λ, m
The first one (*A*)	1317	67	1242÷1461
The second one (*B*)	1623	18	1594÷1651

The values of the wavelength λ and phase speed C can be used to estimate the repetition period of internal waves $T = \lambda/C \approx 24$ min.

Nonlinearity in layered media affects the behavior of internal waves. They acquire the properties of solitary ones and interact with each other as solitons. Their phase speed depends on the amplitude. As a result of dispersion, each leading wave is faster than the next ones [22, 23]. The data given in Table 3 confirm this fact. Since the confidence intervals of the estimates of the phase speeds do not intersect, the result of their difference is statistically guaranteed with a probability of 95%.

Table 3

Phase speeds of the waves *C*

Fronts	Front shift ΔL, m	Average value of phase speed $\overline{C}$, cm/s	Phase speed dispersion σ_C, cm/s	95% confidential interval C, cm/s
Southern (leading) (*s*)	3157	109	1	106÷110
Northern (*n*)	2845	98	2	97÷102

The observed difference in the propagation speeds of the considered internal waves is a sign of their nonlinearity [24]. They can be identified as solitary internal waves, or solitons. For them, the concept of "wavelength" is not defined, and the parameter corresponding to the distance between successive fronts is called the horizontal dimension.

Due to the difference in the speeds of wave crests, the horizontal dimension ("wavelength") between them increases with time (see Table 2). In this case, the redshift $z = \frac{\Delta\lambda}{\lambda}$ is a dimensionless quantity that characterizes the relative increase in the "wavelength" of the leading soliton, is $z \approx 0.23$, and the redshift rate $\Delta z/\Delta t \approx 8{\cdot}10^{-5}$ s^{-1}. Similar facts of a decrease in the horizontal size of the wave with distance from the leading crest are known and were observed earlier, for example, in [25].

Curvature of wave fronts

Parametrically set equidistantly tabulated spatial coordinates of the wave extrema $y(l)$ and $x(l)$ were obtained above, where l is the linear length of the curve measured from one of its ends. In this case, the curvature of curve K is described by the following expression:

$$K = \frac{|x'y'' - y'x''|}{[(x')^2 + (y')^2]^{3/2}},$$

where x', x'', y', y'' are the first and the second derivatives of x and y with regard to parameter l. The value $R = 1/K$, inverse of the curvature, is the curvature radius.

The median values of the radii of curvature R (km) for each front were as follows: 77.46 (A_s), 18.51 (A_n), 36.56 (B_s), 35.38 (B_n).

For each point {x, y} of the curve, the center of curvature is at the point $\{x + R_x, y + R_y\}$. The components of the radius of curvature R_x and R_y along x and y are defined as follows:

$$R_x = x' \cdot R^2, \quad R_y = y' \cdot R^2.$$

Information about the spatial position of the centers of curvature of wave fronts (at least at the early stages of internal wave formation) can make it possible to judge the probable place of their origin. In Fig. 6, against the background of the depth map (using bathymetric data [26]) the positions of wave fronts, their radii of curvature R, and phase speeds are demonstrated.

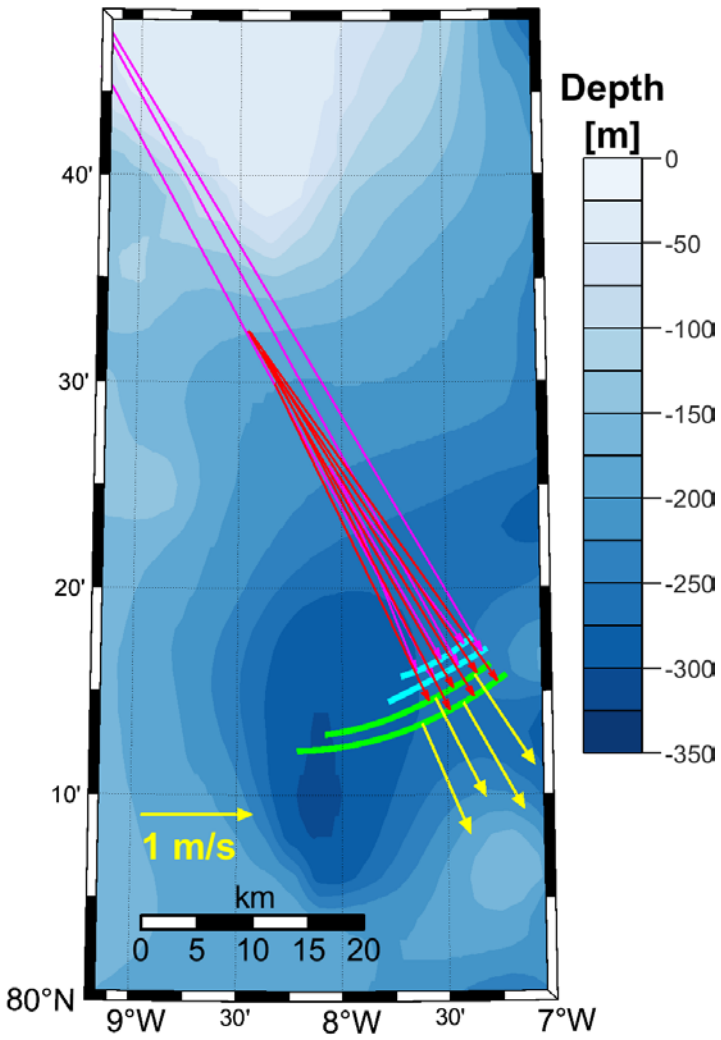

F i g. 6. Position of the internal wave crests, their curvature radii and phase speeds against the background of bathymetry in the region under study

Judging by Fig. 6, the reason for the formation of the considered internal waves can be the interaction of the tide with the underwater bank (80° 45' N, 8° 30' W), the depth above which is less than 20 m.

The satellite data Sentinel-1A, -1B were obtained from the archives of the *Copernicus Open Access Hub* European Marine Forecast Centers (Available at: https://scihub.copernicus.eu).

Conclusion

The paper proposes a method for an objective assessment of the parameters of internal waves based on their manifestations on the ocean surface in the presence of ice floes in the generation area. The data of successive quasi-synchronous soundings of synthetic aperture radars of Sentinel-1A, -1B satellites were used.

The described procedure for masking images made it possible to weed out ice floes and identify IWs. As a result of interpolation and smoothing, the equidistant parametric coordinates of the crest are determined for each individual wave extremum of internal waves.

For the “wavelength” between the crests (the distance between solitons) and the phase speed of propagation of solitary internal waves, statistical estimates of the mean values and dispersions are made. The repetition period of internal waves is calculated. The fact that the first (leading) front propagates faster is confirmed, which leads to an increase (redshift) of the “wavelength” between the crests over time. An estimate of the speed of this increase is obtained.

The values of the curvature radii of each wave front are also calculated. The information about the spatial position of the curvature centers of the fronts is used to infer the probable place of generation of the analyzed internal waves.

REFERENCES

1. Rippeth, T.P., Lincoln, B.J., Lenn, Y.-D., Mattias Green, J.A., Sundfjord, A. and Bacon, S., 2015. Tide-Mediated Warming of Arctic Halocline by Atlantic Heat Fluxes over Rough Topography. *Nature Geoscience*, 8, pp. 191-194. doi:10.1038/ngeo2350
2. Morozov, E.G. and Pisarev, S.V., 2004. Internal Waves and Polynya Formation in the Laptev Sea. *Doklady Earth Sciences*, 398(7), pp. 983-986.
3. Czipott, P.V., Levine, M.D., Paulson, C.A., Menemenlis, D., Farmer, D.M. and Williams, R.G., 1991. Ice Flexure Forced by Internal Wave Packets in the Arctic Ocean. *Science*, 254(5033), pp. 832-835. doi:10.1126/science.254.5033.832
4. Zubkova, E.V., Kozlov, I.E. and Kudryavtsev, V.N., 2016. Spaceborne SAR Observations of Short-Period Internal Waves in the Laptev Sea. *Sovremennye Problemy Distantsionnogo Zondirovaniya Zemli iz Kosmosa*, 13(6), pp. 99-109. doi:10.21046/2070-7401-2016-13-6-99-109 (in Russian).
5. Konyaev, K.V., 2000. Internal Tide at the Critical Latitude. *Izvestiya, Atmospheric and Oceanic Physics*, 36(3), pp. 363-375.
6. Morozov, E.G. and Pisarev, S.V., 2002. Internal Tides at the Arctic Latitudes (Numerical Experiments). *Oceanology*, 42(2), pp. 153-161.
7. Morozov, E.G. and Paka, V.T., 2010. Internal Waves in a High-Latitude Region. *Oceanology*, 50(5), pp. 668-674. doi:10.1134/S0001437010050048
8. Alpers, W., 1985. Theory of Radar Imaging of Internal Waves. *Nature*, 314, pp. 245-247. doi:10.1038/314245a0
9. Bakhanov, V.V., Zuev, A.L., Marov, M.N. and Pelinovskii, E.N., 1989. Influence of Internal Waves on the Characteristics of Microwave Signals Scattered by the Sea Surface. *Izvestiya of*

the Academy of Sciences of the USSR. Atmospheric and Oceanic Physics, 25(4), pp. 387-395 (in Russian).

10. Kudryavtsev, V., Kozlov, I., Chapron, B. and Johannessen, J.A., 2014. Quad-Polarization SAR Features of Ocean Currents. *Journal of Geophysical Research: Oceans*, 119(9), pp. 6046-6065. doi:10.1002/2014JC010173
11. Hong, D.-B., Yang, C.-S. and Ouchi, K., 2015. Estimation of Internal Wave Velocity in the Shallow South China Sea Using Single and Multiple Satellite Images. *Remote Sensing Letters*, 6(6), pp. 448-457. doi:10.1080/2150704X.2015.1034884
12. Liu, B., Yang, H., Ding, X. and Li, X., 2014. Tracking the Internal Waves in the South China Sea with Environmental Satellite Sun Glint Images. *Remote Sensing Letters*, 5(7), pp. 609-618. doi:10.1080/2150704X.2014.949365
13. Tensubam, C.M., Raju, N.J., Dash, M.K. and Barskar, H., 2020. Estimation of Internal Solitary Wave Propagation Speed in the Andaman Sea Using Multi-Satellite Images. *Remote Sensing of Environment*, 252, 112123. doi:10.1016/j.rse.2020.112123
14. Kozlov, I.E., Zubkova, E.V. and Kudryavtsev, V.N., 2017. Internal Solitary Waves in the Laptev Sea: First Results of Spaceborne SAR Observations. *IEEE Geoscience and Remote Sensing Letters*, 14(11), pp. 2047-2051. doi:10.1109/LGRS.2017.2749681
15. Kozlov, I.E. and Mikhaylichenko, T.V., 2021. Estimation of Internal Wave Phase Speed in the Arctic Ocean from Sequential Spaceborne SAR Observations. *Sovremennye Problemy Distantsionnogo Zondirovaniya Zemli iz Kosmosa*, 18(5), pp. 181-192. doi:10.21046/2070-7401-2021-18-5-181-192 (in Russian).
16. Kozlov, I.E., Kudryavtsev, V.N., Zubkova, E.V., Zimin, A.V. and Chapron, B., 2015. Characteristics of Short-Period Internal Waves in the Kara Sea Inferred from Satellite SAR Data. *Izvestiya, Atmospheric and Oceanic Physics*, 51(9), pp. 1073-1087. doi:10.1134/S0001433815090121
17. Zimin, A.V., Kozlov, I.E., Atadzhanova, O.A. and Chapron, B., 2016. Monitoring Short-Period Internal Waves in the White Sea. *Izvestiya, Atmospheric and Oceanic Physics*, 52(9), pp. 951-960. doi:10.1134/S0001433816090309
18. Ivanov, V.A., Shul'ga, T.Ya., Bagaev, A.V., Medvedeva, A.V., Plastun, T.V., Verzhevskaya, L.V. and Svishcheva, I.A., 2019. Internal Waves on the Black Sea Shelf near the Heracles Peninsula: Modeling and Observation. *Physical Oceanography*, 26(4), pp. 288-304. doi:10.22449/1573-160X-2019-4-288-304
19. Bondur, V.G., Morozov, E.G. and Grebenuk, U.V., 2006. [Radar Observation and Numerical Modeling of Internal Tidal Waves off the Coast of the Northwest Atlantic]. *Sovremennye Problemy Distantsionnogo Zondirovaniya Zemli iz Kosmosa*, 3(2), pp. 21-29 (in Russian).
20. Otsu, N., 1979. A Threshold Selection Method from Gray-Level Histograms. *IEEE Transactions on Systems, Man, and Cybernetics*, 9(1), pp. 62-66. doi:10.1109/TSMC.1979.4310076
21. Cleveland, W.S., 1979. Robust Locally Weighted Regression and Smoothing Scatterplots. *Journal of the American Statistical Association*, 74(368), pp. 829-836. doi:10.1080/01621459.1979.10481038
22. Serebryany, A.N., 1993. Manifestation of Soliton Properties on Internal Waves on a Shelf. *Izvestiya, Atmospheric and Oceanic Physics*, 29(2), pp. 229-238.
23. Yong, D.H. and LeVeque, R.J., 2003. Solitary Waves in Layered Nonlinear Media. *SIAM Journal on Applied Mathematics*, 63(5), pp. 1539-1560. doi:10.1137/S0036139902408151
24. Sabinin, K.D. and Serebryanyi, A.N., 2007. "Hot Spots" in the Field of Internal Waves in the Ocean. *Acoustical Physics*, 53(3), pp. 357-380. doi:10.1134/S1063771007030128
25. Ródenas, J.A. and Garello, R., 1997. Wavelet Analysis in SAR Ocean Image Profiles for Internal Wave Detection and Wavelength Estimation. *IEEE Transactions on Geoscience and Remote Sensing*, 35(4), pp. 933-945. doi:10.1109/36.602535

26. Jakobsson, M., Mayer, L.A., Bringensparr, C., Castro, C.F., Mohammad, R., Johnson, P., Kettler, T., Accettella, D., Amblas, D. [et al.], 2020. The International Bathymetric Chart of the Arctic Ocean Version 4.0. *Scientific Data*, 7, 176. doi:10.1038/s41597-020-0520-9

About the author:

Aleksandr E. Pogrebnoi, Research Associate, Marine Hydrophysical Institute of RAS (2 Kapitanskaya Str., Sevastopol, 299011, Russian Federation), Ph.D. (Phys.-Math.), **ORCID ID: 0000-0001-9390-7231**, **Scopus Author ID: 7004734095**, **SPIN-code: 1944-6355**, **ResearcherID: GNP-2733-2022**, pogrebok57@mail.ru

The author has read and approved the final manuscript.
The author declares that he has no conflict of interest.